Particle and Gas Flow Modeling of Wall-impinging Diesel Spray under Ultra-high Fuel Injection Pressures

P. Ghadimi[†], M. Yousefifard and H. Nowruzi

Department of Marine Technology, Amirkabir University of Technology, Tehran, Iran

†*Corresponding Author Email: pghadimi@aut.ac.ir*

ABSTRACT

Advanced models of spray breakup and droplet collision are implemented in OpenFOAM code for comparing the flat-wall impinging and free fuel sprays under ultra-high pressure direct injection diesel engines. The non-evaporating spray and ambient gas flow characteristics are analyzed by a combination of Eulerian and Lagrangian methods for continuous and dispersed phase, respectively. Various injection pressures and two different impinging distances are used. Reynolds Averaged Navier Stokes (RANS) equations are solved using standard k-ε turbulence model. Computational domain and grid size are determined based on a mesh study. Numerical results are validated by published experimental data for free and wall-impinging sprays. The robustness and accuracy of the proposed scheme are confirmed by comparing the main characteristics of spray and surrounding gas against published experimental data. To accomplish this, spray shape, penetration and gas velocity vectors are compared with experimental data and insightful understanding of the spray characteristics are provided. In comparison with free spray, tip penetration has been limited in impinging sprays. Turbulent flow in impinging sprays leads to more induced air motion. Also, impinging spray leads to more pushed-out gas velocity. The obtained results indicate that the numerical findings are generally in good agreement with experimental data in case of ultra-high injection pressures and micro-hole injectors.

Keywords: Wall-impinging spray; Free diesel spray; Ultra-high injection pressure; OpenFOAM.

1. INTRODUCTION

Direct injection (DI) diesel engines have been used considerably as the power source of ships and vehicles. Fuel injection process is the main effective parameter on the engine performance that can lead to higher efficiency and lower emission. Diesel spray simulation is rather complicated because it involves multiple phase transition, fuel atomization, evaporation and combustion. Moreover, it is a transient process in a very short duration. Especially, increasing the injection pressure leads to higher surrounding gas velocities and probability of the wall impinging. There have been numerous studies on the investigation of spray and induced air motion characteristics (Raghu and Nallusamy, 2015). Experimental inspection of the biodiesel and diesel spray characteristics for ultra-high injection pressure up to 300 MPa has been carried out by Wang *et al*. (2010). Wall-impinging sprays have been experimentally studied by Liu *et al*. (2012). They used three kinds of impingement walls in spark-ignition direct injection (SIDI) CNG engines. Their study showed that CNG-air mixture can be easily formed after spray-wall impingement and the ignition probability was also improved. Zhang *et al*. (2008) experimentally investigated the effects of colliding spray with the piston cavity shape walls. They used micro-hole nozzle under ultra-high injection pressures. Also, penetration and evaporation of the diesel sprays injected through a group-hole nozzle with conventional single-hole nozzle sprays have been experimentally compared by Moon *et al*. (2011). They used various engine loads and wall impinging conditions of direct injection diesel engines. Cardenas *et al*. (2008) experimentally studied the interaction of spray-wall and clustered sprays under conditions relevant for diesel engines. Gao *et al*. (2009) experimentally investigated the flame structure of wall-impinging diesel sprays injected by group-hole nozzles in a constant-volume combustion vessel at experimental conditions typical of a diesel engine. Recently, Zhu *et al*. (2014) carried out an experimental study on flow fields of fuel droplets and ambient gas of free diesel spray and flat wall impinging spray. Their experimental data is used to validate the results of the current study.

On the other hand, there have been significant numbers of numerical studies on spray modeling of wall-impinging. Gavaises *et al.* (1996) presented a model for diesel spray wall impact and assessed it against experiments for a number of test cases. Shim *et al.* (2008) numerically studied the atomization, vaporization, and wall impingement process of hollow-cone fuel spray from high-pressure swirl injectors under various ambient temperature conditions. In recent years, an increasing interest has been observed to simulate two impinging sprays (Ko *et al.*, 2003; Ashgriz *et al.*, 2001; Li and Ashgriz, 2006). Ghasemi *et al.* (2014) conducted numerical simulation of twin impinging sprays using ANSYS fluent. Recently, open source codes have been utilized as efficient methods for simulation of diesel spray by many researchers. New submodel could be added to the default sub-routine of these codes. As a result, these toolboxes have been developed based on new findings in the field of breakup and collision models. In this context, KIVA and OpenFOAM have become the most popular codes in the field of IC engines. Accordingly, there have been many studies in this field that have used OpenFOAM code (Ghadimi *et al.*, 2016 a,b; Vuorinen *et al.*, 2011 , Nowruzi *et al.*, 2014 and Yousefifard *et al.*, 2015).

In the current study, advanced sub-models in OpenFOAM are utilized for modeling the breakup and collision process under ultra-high injection pressure. Wall-impinging spray is analyzed and compared with free spray. Different studies have been conducted in simulation of free spray and twin impinging sprays under ultra-high pressures. Experimental data presented by Zhu *et al.* (2014) is used as a benchmark case for validating the numerical simulation of ultra-high pressure impinging spray. Velocity vector distribution is presented to characterize spray gas entrainment. The main innovative part of the current paper is investigation of the effects of impinging distance and injection pressure of ultra-high the injection pressure diesel spray.

2. GOVERNING EQUATIONS

Continuous phase is modeled using Navier-Stokes (NS) equations. Also, the dispersed phase is described by Lagrangian Particle Tracking (LPT) scheme.

2.1 Navier-Stokes Equations

Navier-Stokes equations are described by the conservation of mass and momentum equations (Stiesch, 2003) as in

$$\frac{\partial \rho}{\partial t} + \frac{\partial}{\partial x_j}\left(\rho u_j\right) = 0 \tag{1}$$

$$\frac{\partial}{\partial t}\left(\rho u_i\right) + \frac{\partial}{\partial x_j}\left(\rho u_j u_i\right) = -\frac{\partial P}{\partial x_i} + \frac{\partial}{\partial x_j}\left(\tau_{ij} + \tau_{ij}^{\ R}\right) \tag{2}$$

where $u = \left(u_1, u_2, u_3\right)$ is the velocity vector, $P \equiv p + \rho g z$ is the modified pressure variable, ρ is

the flow density and $\tau = \tau_{ij}$ is the resolved stress tensor which can be defined as follows:

$$\tau_{ij} = -p\delta_{ij} + 2\mu S_{ij} , \tag{3}$$

Here, S_{ij} as represents the rate of strain tensor which is defined as

$$S_{ij} = \frac{1}{2}\left(\frac{\partial u_i}{\partial x_j} + \frac{\partial u_j}{\partial x_i}\right). \tag{4}$$

Moreover, $\tau_{ij}^{\ R}$ in Eq.(2) is

$$\tau_{ij}^{\ R} = -\rho\overline{u_i' u_j'}. \tag{5}$$

2.2 Droplet Motion

Based on Lagrangian viewpoint, the dispersed phase is described by Newton's equation of motion as in:

$$\frac{1}{6}\rho_p \pi d^3 \frac{du_p}{dt} = \frac{1}{2}\left(u_g - u_p\right)\left|u_g - u_p\right|\rho_g C_D \frac{\pi d^2}{4} \tag{6}$$

where u_p is the particle velocity, u_g is gas velocity that is interpolated on the particle position from the adjacent cells and C_D is the droplet drag coefficient that can be defined by:

$$C_D = \begin{cases} \frac{24}{\mathrm{Re}_p}\left(1 + \frac{1}{6}\mathrm{Re}_p^{2/3}\right), & \mathrm{Re}_p < 1000 \\ 0.424, & \mathrm{Re}_p \geq 1000 \end{cases} \tag{7}$$

2.3 Droplet Breakup

The spray atomization process can be divided into two main steps; primary and secondary breakup. Blob model (Reitz and Diwakar, 1987) has been used for modeling the primary breakup. Based on this model, the diameter of injected blobs right after the injector nozzle is equal to the nozzle diameter and number of drops injected per unit time is determined from the flow rate profile. On the other hand, secondary breakup process is described by aerodynamic stripping of smaller droplets from larger droplets (Kelvin-Helmholtz (KH) instability) or disintegration of larger droplets into smaller ones due to the effect of normal stresses (Rayleigh-Taylor (RT) instability).

In this paper, KHRT hybrid breakup model (Reitz, 1987) has been used. This model is the combination of KH wave model and RT instabilities at the droplet surface. RT instabilities appear when the acceleration is normal to the interface of two fluids with different densities. Similar to the KH instabilities, the wavelength and the growth rate of the fastest growing wave can be obtained through linear stability analysis. Liquid viscosity and gravity are neglected when performing these calculations.

In the KH model, Ω_{KH} and Λ_{KH} are the wavelength and growth rate of the fastest growing wave on the surface of the liquid jet defined as follows:

$$\Omega_{KH}\left[\frac{\rho_l r_0^3}{\sigma}\right]^{0.5} = \frac{0.34 + 0.38 \cdot We_g^{1.5}}{(1+Oh)(1+1.4 \cdot T^{0.6})} \qquad (8)$$

$$\frac{\Lambda_{KH}}{r_0} = 9.02 \frac{(1+0.45 \cdot Oh^{0.5})(1+0.4 \cdot T^{0.7})}{(1+0.865 \cdot We_g^{1.67})^{0.6}} \qquad (9)$$

where:

$$Oh = \frac{\sqrt{We_l}}{Re_l}$$

$$T = Oh\sqrt{We_g}$$

$$We_g = \frac{\rho_g u_{rel}^2 r_0}{\sigma} \qquad (10)$$

$$We_l = \frac{\rho_l u_{rel}^2 r_0}{\sigma}$$

Here, We, Re, Oh and T are dimensionless numbers of Weber, Reynolds, Ohnesorge, and Taylor, respectively. In addition, u_{rel} is the relative speed between droplets and ambient gas. The droplet radius before breakup and surface tension are also shown by r_0 and σ, respectively. Indices l and g for density and Weber number are representative of liquid fuel and ambient gas, respectively.

Growth rate of the fastest growing wave (Ω_{RT}) and the corresponding wavelength (Λ_{RT}) in the RT model are written as

$$\Omega_{RT} = \sqrt{\frac{2}{3\sqrt{3\sigma}} \frac{[a(\rho_l - \rho_g)]^{1.5}}{\rho_l - \rho_g}}, \qquad (11)$$

$$\Lambda_{RT} = C_3 2\pi \sqrt{\frac{3\sigma}{a(\rho_l - \rho_g)}} \qquad (12)$$

Here, a is the acceleration of the droplet at the interface of two liquids and constant parameter C_3 is considered to be 5.5 (Reitz, 1987).

Drops can only break if the wavelength (Λ_{RT}) is smaller than their diameters.

In the KH-RT model, the KH model is applied in vicinity of the injector nozzle and RT is employed at certain distance from the nozzle. This consideration is due to the fast devaluation of droplet diameter phenomena near the nozzle by the use of RT model (Ghadimi *et al.*, 2016 c; Nowruzi *et al.*, 2016 b).

2.4 Droplet Collision

There exist two different models for simulation of the droplet collision. The O'Rourke collision model is based on calculation of collision probability for two droplets in the same cell (O'Rourke and Bracco, 1980). O'Rourke collision model is strongly grid dependent. There is also a new collision model presented by Nordin (2001) that calculates the path of all parcels and collides that will intersect within the same time step. As a result, new algorithm has been defined for calculation of parcels paths. These procedures reduce the computational load of the collision modeling. In the current paper, Nordin collision model has been implemented.

3. COMPUTATIONAL MODEL

The conducted simulations in the present study have been carried out based on the conditions involved in experimental study of Zhu *et al.* (2012). Table 1 shows the fuel specifications and operating conditions.

Table 1 Simulation data

Injection duration (ms)	2.2
Fuel Density (kg/m³)	830
Fuel Viscosity (mm²/s)	3.36
Fuel Surface tension (mN/m)	25.5
Ambient gas	Nitrogen
Ambient gas temperature (K)	300
Ambient gas density (kg/m³)	15(300K, 1.4MPa)
Nozzle diameter (mm)	0.08
Injection pressure (MPa)	100, 200 and 300
Impinging distance (mm)	30, 40

The mentioned simulations have been carried out using SprayFoam solver of OpenFOAM 2.1.1 code. Pressure-velocity coupling has been carried out using PISO algorithm (Ferziger and Peric, 2002), and Favre time averaging is applied to velocity components. Also, the standard $k - \varepsilon$ turbulence model (Jones and Launder, 1972) is utilized in RANS modeling scheme.

Based on a grid independency study, 1.0×10^6 cells are applied to the domain of $(50 \times 50 \times 100 \text{ mm}^3)$ size for the free spray. Also, impinging sprays are modeled using a domain size of $(80 \times 80 \times 40 \text{ mm}^3)$ and $(80 \times 80 \times 30 \text{ mm}^3)$. The schematic view of domain geometry is presented in Fig. 1.
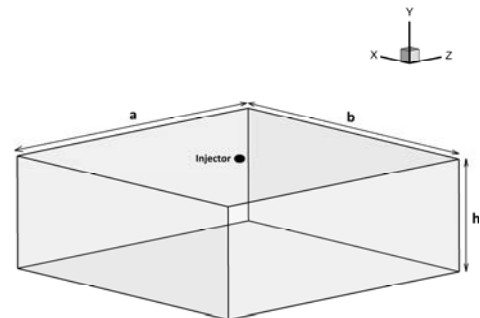

Fig. 1. Schematic view of the computational domain.

Injection flow rate is the main boundary condition for the current simulation. Fuel flow rate can be determined based on fuel and ambient pressure and nozzle diameter through theoretical equations. In addition, experimental data related to the flow rate is presented by Zhu *et al.* (2012). Therefore, in the current study, these values have been used as boundary conditions for the injector. Fig. 2 shows the fuel flow rate vs. time under injection pressures of 100, 200 and 300 MPa presented by Zhu *et al.* (2012).
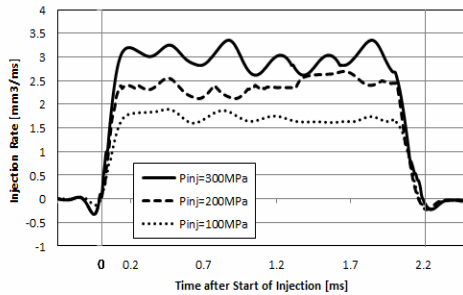
Fig. 2. Injector flow rate (Zhu *et al.*, 2012).

4. RESULT AND DISCUSSION

4.1 Global Characteristics

Figure 3 shows the comparison of numerical spray droplet cloud under the fuel injection pressure of 100 MPa and two nozzle-wall distances.
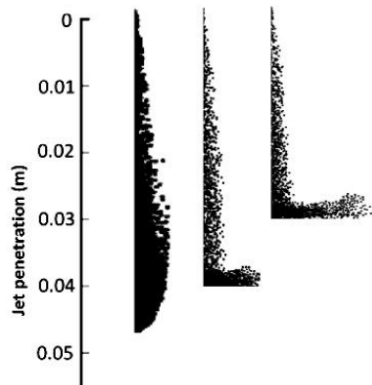
**Fig. 3. Comparison of the simulated spray shapes of free and wall-impinging sprays (Pinj=100MPa, t=1.0ms).**

It is quite evident that spray shape in the region prior to the wall-impinging has similar tendency for the free and impinging spray. After spray-wall impingement, liquid film has been formed in vicinity of the wall and a fraction of spray droplets rebound from the wall and enter the surrounding gas.

Spray penetration lengths of free and impinging spray under different injection pressures are displayed and compared against experimental results in Fig. 4. The wall-impinging spray penetration is defined as the summation of impinging distance and half of the radial spray

length (see Fig. 7). It is evident that the penetration length of the free spray is larger than the wall impinging sprays. Similar to the results of free spray, the spray height is increased with time. Higher injection pressure leads to increase in the spray length along the radial direction. Also, increasing the injection pressure leads to higher values of tip penetration. The enhanced penetration with the impinging of 30 mm and 40 mm is illustrated in Fig. 4.
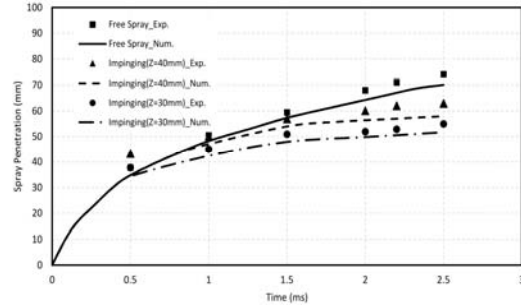
(a)
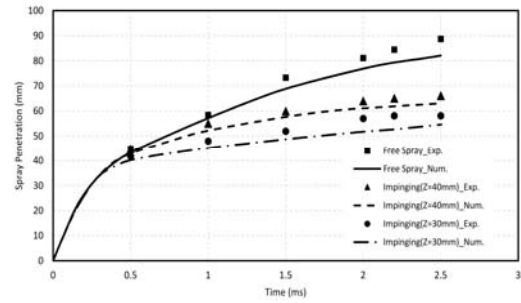
(b)
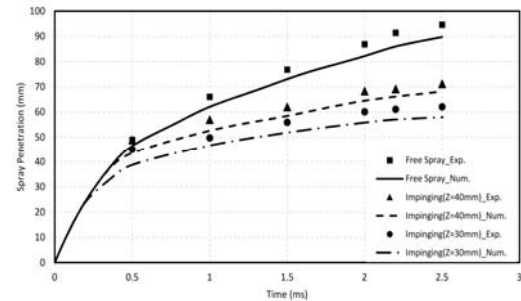
(c)

Fig. 4. Comparison of spray tip penetration length for the free and two different wall-impinging sprays at: (a) Pinj=100MPa, (b) Pinj=200MPa, and (c) Pinj=300MPa.
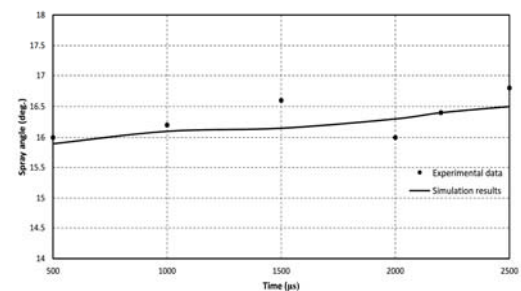

Fig. 5. Spray cone angle of the free spray VS time (Pinj=100MPa).
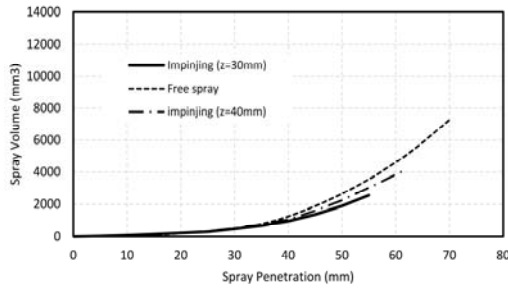
Fig. 6. Spray volume VS penetration length (Pinj=100MPa).

Flow of Spray Droplets

Flow of Ambient Gas at Periphery of Spray

(a)

Flow of Spray Droplets
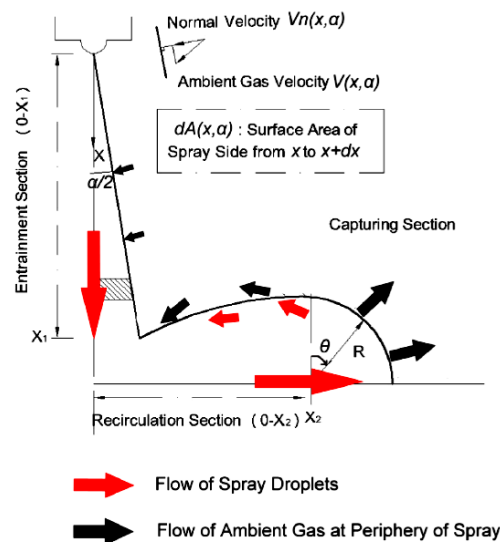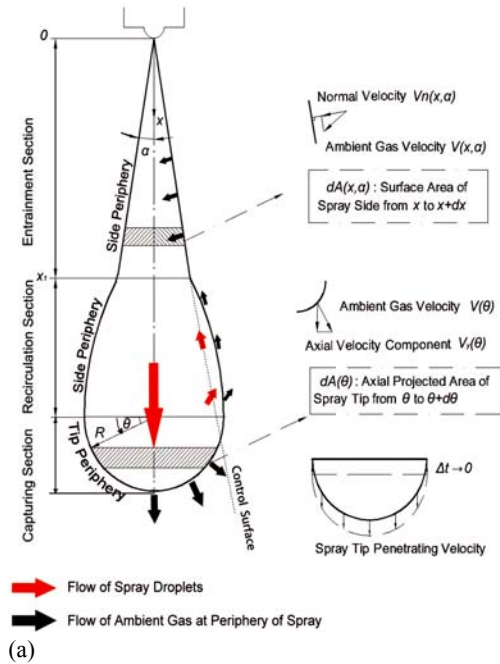
Flow of Ambient Gas at Periphery of Spray

(b)

Fig. 7. Definition of the velocity components, sections around the spray periphery of (a) free and (b) impinging sprays (Zhu *et al.*, 2012, 2014).

Figure 5 presents the variation of spray cone angle at different times after the start of injection for the free spray under 100MPa of injection pressure. Spray angle is measured based on the radial distance at the axial location of 40 mm. It is impossible to display spray cone angle in case of wall-impinging sprays. However, there are no changes in the spray cone angle before wall impingement. On the other hand, increasing the injection pressure has little influence on the free spray cone angle (Yousefifard *et al.*, 2014a).
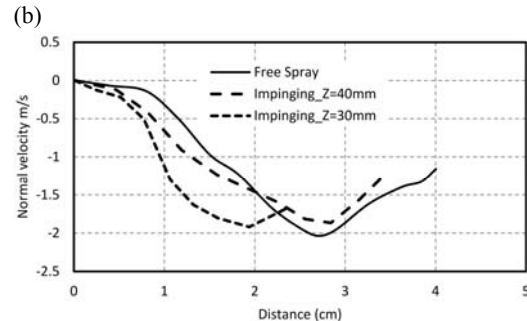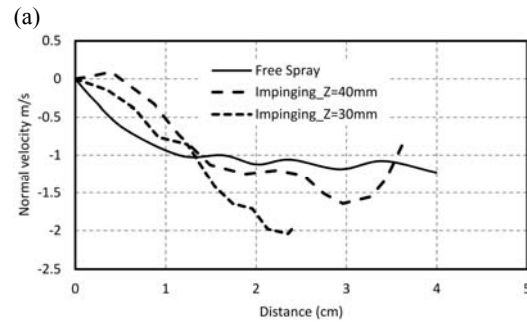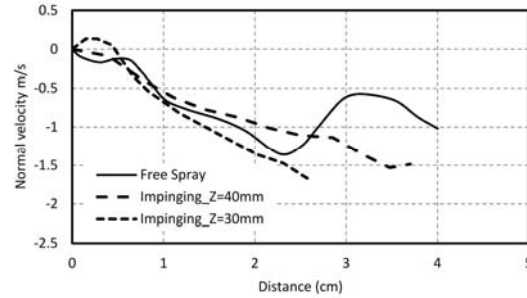

(a)

(b)

(c)

Fig. 8. Spatial distribution of normal velocity along the control surface at: (a) Pinj=100MPa, (b) Pinj=200MPa, and (c) Pinj=300MPa.

Other spray characteristics are related to spray penetration and angle (Yousefifard *et al.*, 2014b). Hence, as evident in Fig. 6, the spray volume is shown to have the same tendency as the spray penetration.

4.2 In-Cylinder Gas Motion

Zhu *et al.* (2014) proposed a quantitative method to analyze the wall-impinging spray induced ambient gas flow. The gas mass flow rate is calculated based on the model presented in Fig. 6. A control surface is drawn along the spray expansion angle from the nozzle tip and extends to far field straightly (as shown in Fig. 6). Normal velocity is defined as the gas velocity component perpendicular to the control surface.
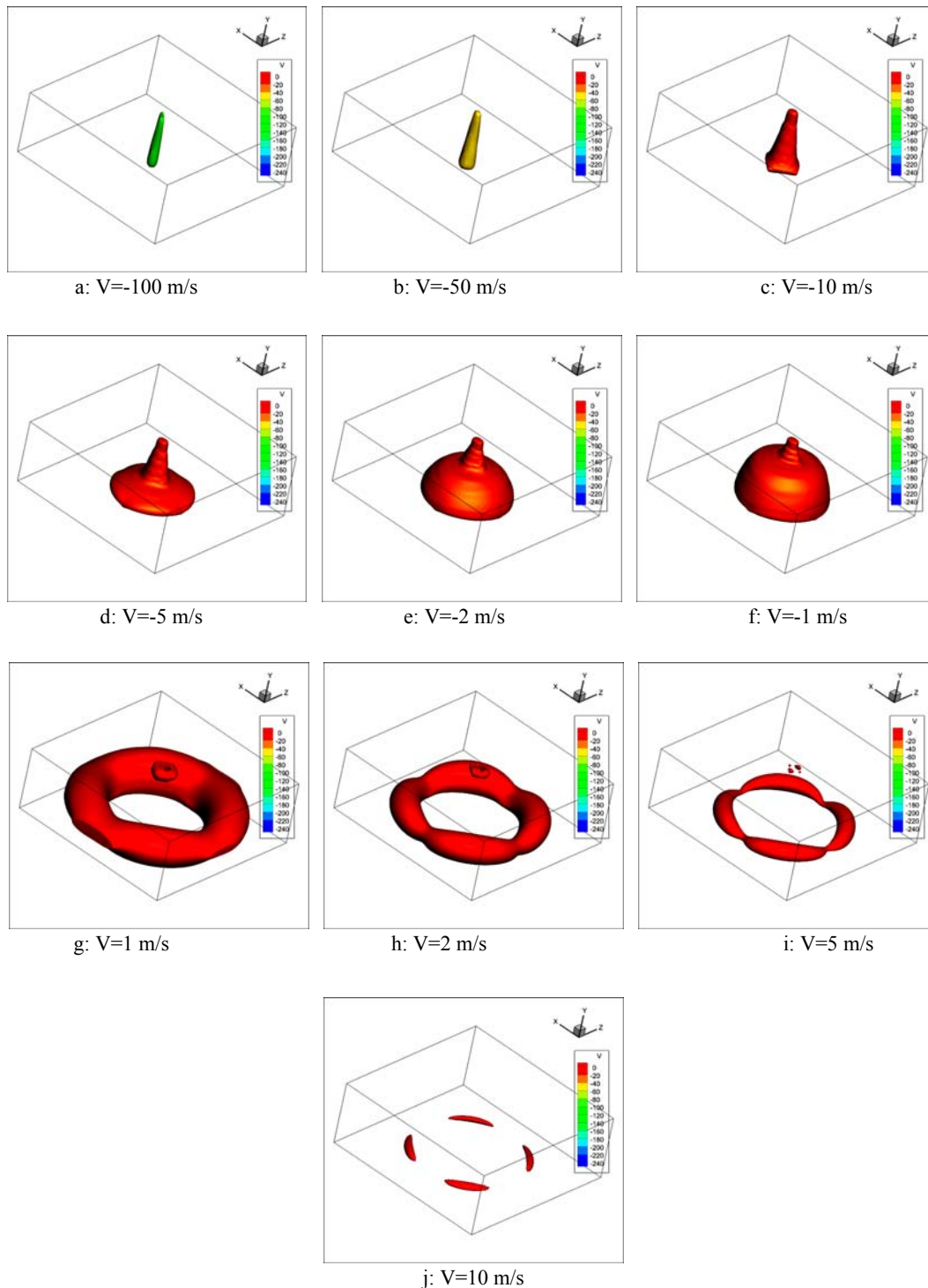
a: V=-100 m/s

b: V=-50 m/s

c: V=-10 m/s

d: V=-5 m/s

e: V=-2 m/s

f: V=-1 m/s

g: V=1 m/s

h: V=2 m/s

i: V=5 m/s

j: V=10 m/s

Fig. 9. The iso-surface plots of velocity along Y axis (Pinj=200MPa, t=1.0 ms).

As illustrated in Fig. 7, the gas field around the spray is divided into three sections in both free and impinging sprays. These three main zones have been stated by Sepret *et al.* (2010). In entrainment zone, the gas velocity vectors move into the spray. After that, gas velocity vectors seem to have recirculated in the wake of leading head. Finally, in gas pushed out zone, the gas velocity vectors are pushed outward by the spray tip. The normal velocity along the spray side periphery of the free and the impinging sprays under different injection pressures at t=1.0ms are presented in Fig. 8. In both free and impinging sprays, normal velocity is the same near the nozzle tip region. After that, the normal velocity of the impinging spray increases. Reduction of the impinging distance further increases the normal velocity. In case of free spray at low injection pressure, a decrease in velocity

magnitude has been observed. Increasing the particle diameter leads to high aerodynamic force and therefore, particle velocity has been significantly reduced.

Axial velocity (velocity component along the injector axis) of the surrounding gas is analyzed in Fig. 9. The iso-surface plots of axial velocity show that direction of velocity components change toward the injector hole due to the turbulent flow around the spray. Maximum velocity values are detected at the core of spray, where the initial particle velocity has not been affected by the drag force. Streamlines of induced air motion present another proof of particle motion in the middle of spray (Fig. 10). Negative values are along the injection direction. It is evident in Fig. 9 that gas velocity components have the same trend toward the injected droplet in vicinity of the spray. However, the direction of gas velocity components changes toward the injector in the field away from the spray.

Also, induced air motion streamlines are presented in Fig. 10. Recirculation of the surrounding air can be observed. Positive magnitude of the vertical velocity is presented in Fig. 9 displays this phenomena.
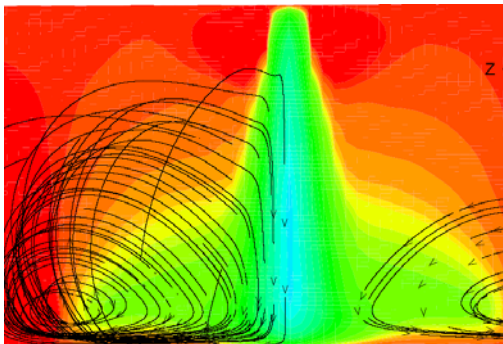

Fig. 10. Streamlines around the spray at XY plane (Pinj=200MPa, t=1.0 ms).

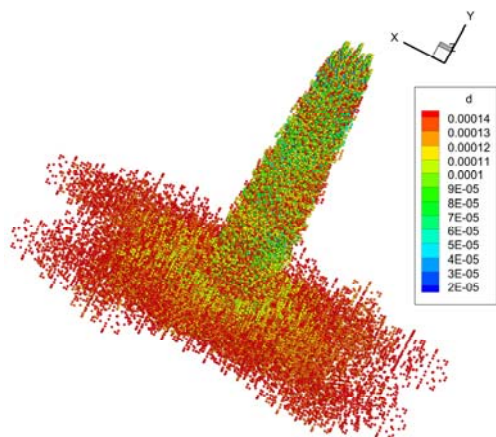**Fig. 11. 3D plot of wall-impinging spray shape and droplet size normalized with respect to the injector diameter (Pinj=200 MPa, t=1.0 ms).**

Finally, 3D plot of droplets cloud of wall-impinging

spray at t=1.0 ms and Pinj= 200 MPa are presented in Fig. 11. In this figure, droplet size is normalized with respect to the injector diameter for better presentation of the spray shape. Wall impingement leads to an increase in the droplet diameter because the droplet coalescence may lead to larger droplet in this area.

Figure 12 (a) shows the gas velocity components in the direction of spray penetration at t=2.0 ms after the start of injection. The angle θ=90° illustrates gas velocity component along the spray penetration at the spray tip (See Fig. 7). Fig. 12 (a) demonstrates that impinging distance has major effect on the gas velocity components. Higher values of the velocity are observed in the case of lower impingement distance. The effects of injection pressure on the velocity vectors along the spray penetration at the spray tip are presented in Fig. 12 (b). It is quite evident that higher injection pressures lead to small increase in the gas velocity at the spray tip.
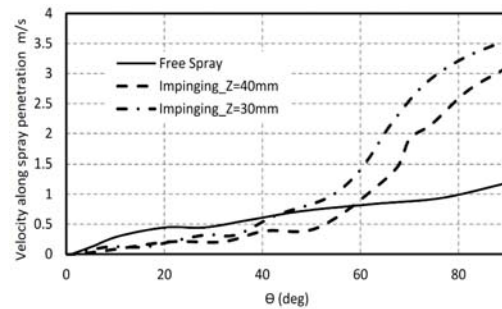
(a)
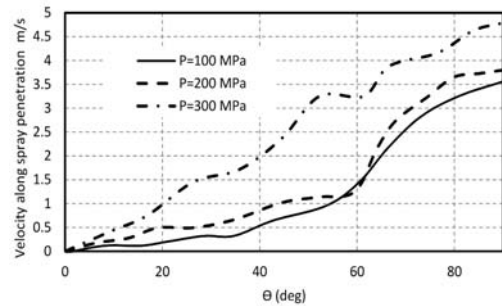
(b)

Fig. 12. Gas velocity distribution along the spray penetration at the spray tip: (a) The effects of impinging distance (Pinj=100 MPa, t=2.0 ms), (b) The effects of injection pressure (t=2.0 ms).

5. CONCLUSION

In the current paper, influence of injection pressure and impinging distance is studied on the non-evaporating and non-reacting ultra-high injection pressure of free and impinging diesel sprays. This is accomplished numerically using the advanced breakup and collision sub-models. OpenFOAM code is implemented and Lagrangian particle tracking scheme is adopted for the liquid droplet modeling and RANS method is used to simulate the continuous gas field. Spray and gas field

characteristics are analyzed. The characteristics of free and impinging sprays are compared against experimental data. Spray penetration and gas entrainment are the main parameters that are compared with experimental data and good agreements are achieved between the obtained numerical results and reported experiment.

The spray characteristics before the wall-impingement are similar to the free spray properties. The sprays are already atomized before reaching the impinging wall. In the impact zone, the spray grows into the radial direction and the spray penetration is limited. On the other hand, flow turbulence leads to more gas pushed-out in the tip zone of the impinging spray. Impingement distance has the main effect on gas velocity at the spray tip. Higher gas velocity vectors at the spray tip are observed in lower impingement distances. On the other side, increasing the injection pressure leads to a slight growth of the gas velocity at the spray tip. Increase in injection pressure in micro-hole nozzles that is used in the current simulation provides larger spray penetration and wall impingement which leads to larger droplet size. It can be concluded that the obtained numerical results in the current study are close to the experimental data in case of free and wall-impinging sprays

REFERENCES

Ashgriz, N., W. Brocklehurst and D. Talley (2001). Mixing mechanisms in a pair of impinging jets. J. Propul. Power 17(3), 736-749.

Cardenas, M., A. Pawlowski, M. Günthera and R. Kneer (2008). Spray-wall interaction of clustered sprays under conditions relevant for diesel engines. ILASS 2008, Como Lake, 8-10.

Ferziger, J. H. and M. Peric (2002). Computational methods for fluid dynamics. Springer.

Gao, J., S. Moona, Y. Zhang, K. Nishida and Y. Matsumoto (2009). Flame structure of wall-impinging diesel fuel sprays injected by group-hole nozzles. Combustion and Flame 156, 1263-1277.

Gavaises, M., A. Theodorakakos and G. Bergeles (1996). Modeling wall impaction of diesel sprays. Int. J. Heat Fluid Flow 17(2), 130-138.

Ghadimi, P. and H. Nowruzi (2016). The effects of heavy fuel oil blend with ethanol, n-butanol or methanol bioalcohols on the spray characteristics. Journal of Applied Fluid Mechanics 9(5), 2413-2425.

Ghadimi, P., H. Nowruzi, M. Yousefifard and M. A. F. Chekab (2017). A CFD study on spray characteristics of heavy fuel oil-based microalgae biodiesel blends under ultra-high injection pressures. *Meccanica 52* (1-2), 153-170.

Ghadimi, P., M. Yousefifard and H. Nowruzi (2016). Applying different strategies within Openfoam to investigate the effects of breakup

and collision model on the spray and in-cylinder gas mixture attribute. Journal of Applied Fluid Mechanics 9(6), 2781-2790.

Ghasemi, A., R. M. Barron and R. Balachandar (2014). Spray-induced air motion in single and twin ultra-high injection diesel sprays. *Fuel 121*, 284-297.

Jones, W. P. and B. E. Launder (1972). The prediction of laminarization with a two-equation model of turbulence. Int. J. Heat Mass Transfer 15, 301–314.

Ko. G. H., S. H. Lee , H. S. Ryou and Y. K. Choi (2003). Development and assessment of a hybrid droplet collision model for two impinging sprays. Atomization Sprays 13(2-3), 251-272.

Li, R., and N. Ashgriz (2006). Characteristics of liquid sheets formed by two impinging jets. Phys. Fluids 18(8).

Liu, Y., J. K. Yeom and S. S. Chung (2012). An experimental study on the effects of impingement-walls on the spray and combustion characteristics of SIDI CNG. J. Mech. Sci. Technol, 26(8).

Moon, S., W. Zhang, K. Nishida, Y. Matsumoto and J. Gao (2011). Development and evaporation of group-hole nozzle sprays under various surrounding and impinging conditions of direct-injection diesel engines. *International Journal of Engine Research 12*(1), 41-57.

Nordin, N. (2001). Complex chemistry modeling of diesel spray combustion. Ph.D thesis, Dept. of Thermo and Fluid Dynamics, Chalmers University of Technology, Goteborg, Sweden.

Nowruzi, H. and P. Ghadimi (2016). Effect of water-in-heavy fuel oil emulsion on the nonreacting spray characteristics under different ambient conditions and injection pressure: a CFD study. *SCIENTIA IRANICA 23*(6), 2626-2640.

Nowruzi, H., P. Ghadimi and M. Yousefifard (2015). Large eddy simulation of ultra-high injection pressure diesel spray in marine diesel engines. *Transactions of FAMENA 38*(4), 65-76.

O'Rourke, P. J. and F. V. Bracco (1980). Modelling of Drop Interactions in Thick Sprays and a Comparison with Experiments. Proc I Mech E 9, 101–116.

Raghu, P. and N. Nallusamy (2015). Study of spray characteristics of biodiesel using dimensionless analysis under non evaporating conditions. Iranian Journal of Science and Technology Transactions of mechanical engineering 39, 389-398.

Reitz, R. D. (1987). Modeling atomization processes in high-pressure vaporizing sprays. Atomization and Spray Technology 3, 309-337.

Reitz, R. D. and R. Diwakar (1987). Structure of high-pressure fuel sprays. SAE; Technical , 870598.

Sepret, V., R. Bazile and M. Marchal (2010). Effect of ambient density and orifice diameter on gas entrainment by a single-hole diesel spray. Exp Fluids 49, 1293-1305.

Shim, Y. S., G. M. Choi and D. J. Kim (2008). Numerical modeling of hollow-cone fuel atomization, vaporization and wall impingement processes under high ambient temperatures. Int. J. Automot. Technol. 9(3), 267-275.

Stiesch, G. (2003). Modeling Engine Spray and Combustion Processes. Springer.

Vuorinen, V., C. Duwig, L. Fuchs and *et al*. (2011). Large-Eddy simulation of a compressible spray using eulerian-eulerian approach. In 24th European Conference on Liquid Atomization and Spray Systems, Estoril, Portugal.

Wang, X., Z. Huang, O. A. Kuti and *et al*.(2010). Experimental and analytical study on biodiesel and diesel spray characteristics under ultra-high injection pressure. Int. J. Heat Fluid Flow 31, 659-666.

Yousefifard, M., P. Ghadimi and H. Nowruzi (2015). Numerical investigation of the effects of chamber backpressure on HFO spray characteristics. Int. J. Automot. Technol 16(2), 339-349.

Yousefifard, M., P. Ghadimi and M. Mirsalim (2014 a). Numerical simulation of biodiesel spray under ultra-high injection pressure using OpenFOAM. Journal of the Brazilian Society of Mechanical Sciences and Engineering.

Yousefifard, M., P. Ghadimi and H. Nowruzi, (2014 b). Three-dimensional LES modeling of induced gas motion under the influence of injection pressure and ambient density in an ultrahigh-pressure diesel injector. *Journal of the Brazilian Society of Mechanical Sciences and Engineering 37*(4), 1235-1243.

Zhang, W., K. Nishida, J. Gao and D. Miura (2008). An experimental study on flat-wall-impinging spray of microhole nozzles under ultra-high injection pressures. In Proceedings of the Institution of Mechanical Engineers, Part D: Journal of Automobile Engineering, 1731-1741.

Zhu, J., K. Nishida and T. Uemura (2014). Experimental study on flow fields of fuel droplets and ambient gas of diesel spray-free spray and flat-wall impinging spray. Atomization Sprays 24(7), 599–623.

Zhu, J., O. A. Kuti and k. Nishida (2012). An investigation of the effects of fuel injection pressure, ambient gas density and nozzle hole diameter on surrounding gas flow of a single diesel spray by the laser-induced fluorescence-particle image velocimetry technique. Int. J. Engine Res. 14.